doi:10.1016/j.jmb.2008.03.058 J. Mol. Biol. (2008) 379, 136–145

JMB

Available online at www.sciencedirect.com

ScienceDirect

ELSEVIER

Zinc Binding Catalytic Domain of Human Tankyrase 1

Lari Lehtiö[1]†, Ruairi Collins[1]†, Susanne van den Berg[1], Andreas Johansson[1], Lars-Göran Dahlgren[1], Martin Hammarström[1], Thomas Helleday[2,3], Lovisa Holmberg-Schiavone[1], Tobias Karlberg[1]* and Johan Weigelt[1]*

[1]*Structural Genomics Consortium, Department of Medical Biochemistry and Biophysics, Karolinska Institutet, S-17177 Stockholm, Sweden*

[2]*Department of Genetics, Microbiology and Toxicology, Stockholm University, S-106 91 Stockholm, Sweden*

[3]*Radiation Oncology and Biology, University of Oxford, Oxford OX3 7LJ, UK*

Received 21 December 2007; received in revised form 20 March 2008; accepted 25 March 2008
Available online 3 April 2008

Edited by G. Schulz

Tankyrases are recently discovered proteins implicated in many important functions in the cell including telomere homeostasis and mitosis. Tankyrase modulates the activity of target proteins through poly(ADP-ribosyl)ation, and here we report the structure of the catalytic poly(ADP-ribose) polymerase (PARP) domain of human tankyrase 1. This is the first structure of a PARP domain from the tankyrase subfamily. The present structure reveals that tankyrases contain a short zinc-binding motif, which has not been predicted. Tankyrase activity contributes to telomere elongation observed in various cancer cells and tankyrase inhibition has been suggested as a potential route for cancer therapy. In comparison with other PARPs, significant structural differences are observed in the regions lining the substrate-binding site of tankyrase 1. These findings will be of great value to facilitate structure-based design of selective PARP inhibitors, in general, and tankyrase inhibitors, in particular.

Keywords: tankyrase; poly(ADP-ribose) polymerase; inhibitor design; zinc

Introduction

Tankyrase (TRF1-interacting ankyrin-related ADP-ribose polymerase, TNKS) was first identified in 1998[1] and found to interact with telomeric repeat binding factor (TRF1), a protein that binds to and protects telomeric DNA. The human genome encodes two tankyrases, TNKS-1 and TNKS-2, which have high sequence identity (Fig. 1). Tankyrases belong to the poly(ADP-ribose) polymerase (PARP) family of proteins that all share a catalytic PARP domain. PARP activity, poly(ADP-ribosyl)ation or PARsylation of acceptor proteins, is emerging as an important regulatory mechanism in the cell and is gaining increasing attention in the scientific literature. The most studied function of PARP enzymes is their function in the DNA repair machinery (PARP-1 and PARP-2); however, PARPs are involved in many biological processes, and specific functions are yet to be assigned to several members of the family.[3] In addition to the PARP domain [residues 1091–1313; National Center for Biotechnology Information (NCBI) ID NP_003738.2], TNKS-1 carries an ankyrin repeat domain (residues 208–945) that facilitates binding to TRF1 and other interaction partners,[4] a sterile alpha motif domain (residues 1028–1087) that is required for homo- and hetero-oligomerization,[5,6] and an N-terminal HPS domain consisting of homopolymeric tracts of His, Pro and Ser (Fig. 1).[1]

*Corresponding authors. E-mail addresses: tobias.karlberg@ki.se; johan.weigelt@ki.se.

† L.L. and R.C. contributed equally to this work.

Present address: L. Holmberg-Schiavone, Structural Chemistry Laboratory, AstraZeneca R&D, Mölndal, Sweden.

Abbreviations used: TNKS, tankyrase; TRF1, telomeric repeat binding factor; PARP, poly(ADP-ribose) polymerase; PAR, poly(ADP-ribose); PARsylation, poly(ADP-ribos)ylation; NI, nicotinamide; AD, adenosine; TCEP, tris(2-carboxyethyl)phosphine.

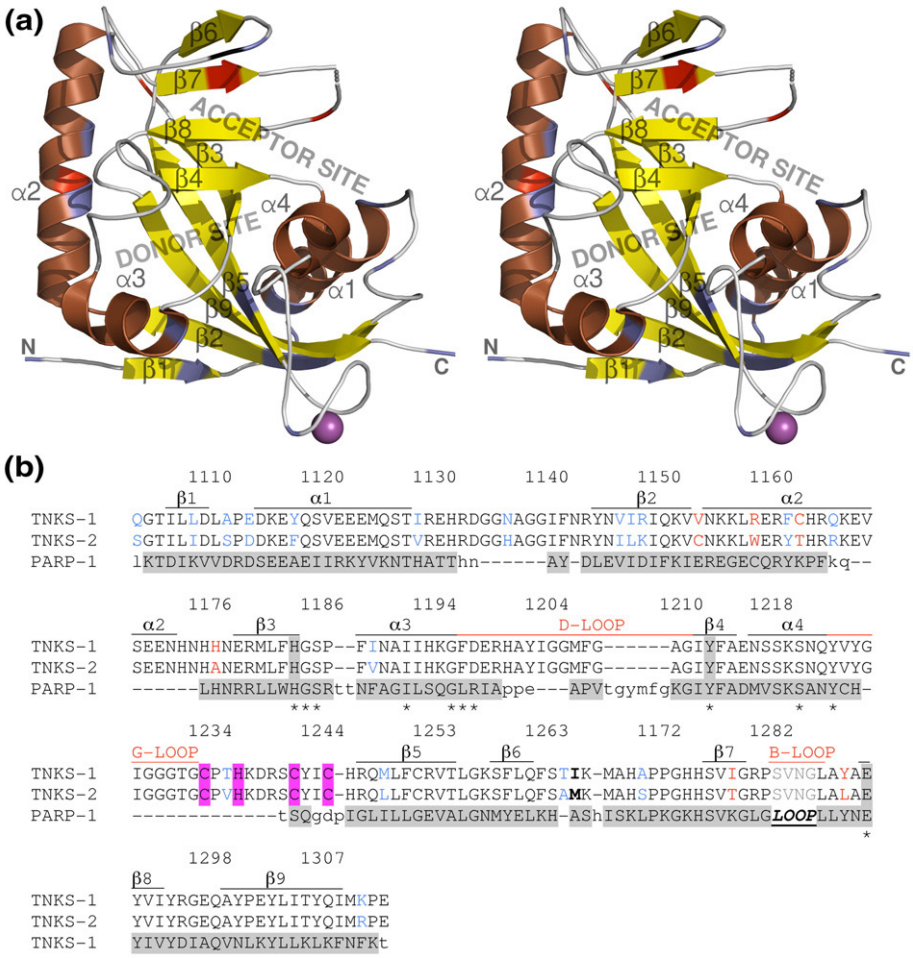

Fig. 1. Structure of the catalytic domain of TNKS-1. (a) Stereo view of the catalytic domain. Residues that are not conserved between TNKS-1 and TNKS-2 are colored red. The Zn ion is shown as a sphere. The disordered loop 1283–1286 is shown as a dashed line. The donor and acceptor NAD^+ binding sites are labeled as well as secondary-structure elements and N- and C-termini. Amino acid difference between the reported structure in comparison with NP_003738 (NCBI ID), M1266I, is colored black. (b) Sequence alignment of the TNKS-1 and TNKS-2 PARP domains and structural alignment with human PARP-1. Identical residues are uncolored, similar are colored blue and unconserved in red. The residues binding the zinc ion are highlighted in magenta and the PARP signature sequence (HYE) is shaded grey in all sequences. All the residues interacting with NAD in the PARP-1 model[2] are marked with a *. B-, D- and G-loops referred to in the text are labeled (sequence of PARP-1 B-loop is not shown). Residues used in the alignment are in gray-shaded capital letters. Residues of PARP-1, which were not aligned, are in small letters. M1266I change is in bold letters. The secondary structural elements are labeled as in (a). The numbering corresponds to TNKS-1 sequence.

TNKS-1 localizes to many sites within the cell such as telomeres, spindle poles and cytoplasmic membrane compartments.[4] Its catalytic activity has been shown to be required also for progression through mitosis.[7,8] However, the most documented function of TNKS-1 is its involvement in telomere homeostasis.[1,4] Human telomerase is a reverse transcriptase that maintains telomere length by adding telomeric repeats to the ends of chromosomes.[9] Telomeres are protected by a nucleoprotein complex referred to as the shelterin complex (de Lange[10] and references therein). PARsylation of TRF1 by TNKS-1 disrupts the shelterin complex and exposes the telomeric DNA. Telomerase can then access the DNA and add telomeric repeats. In normal cells, where progressive telomere shortening limits the number of cell divisions before cells reach replicative senescence, telomerase activity cannot be detected or is very low.[11] On the other hand, telomerase activity is high in germ cells and several cancer cells.[12–15] Inhibition of telomerase activity provides an exciting opportunity for development of novel cancer therapies and has been a field of intense study over the last 10 years.[16] As a positive regulator of telomerase, TNKS-1 is an attractive target for drug development, and inhibition of the TNKS-1 PARP activity has been demonstrated to work synergistically with direct telomerase inhibition to enhance telomere shortening.[17] Several small−molecule PARP inhibitors are available and at least six clinical trials with selective PARP-1 inhibitors for the treatment of various oncology conditions are ongoing or due to be started.[18] This shows great promise for the future development of tankyrase inhibitors.

Here we report the crystal structure of the PARP-domain of TNKS-1, which represents the first

structure of a tankyrase from any species. The catalytic domain of TNKS-1 is structurally homologous to the PARP-proteins reported earlier, but the structure displays distinct features of potential biological and pharmaceutical importance. In particular, the donor NAD^+ binding site of TNKS-1 is not conserved in other members of the PARP family, which will be of importance for the development of selective tankyrase inhibitors. The structure also reveals that TNKS-1 contains a zinc-binding motif that has not been reported or predicted before. The short zinc-binding motif may be involved in protein–protein and/or protein–DNA interactions and thus in the activation of the PARP-reaction catalyzed by tankyrases.

Results and Discussion

Overall structure

The structure of the PARP domain of human TNKS-1 comprises residues 1104–1314 and consists of two central β-sheets consisting of five (β1, β2, β3, β5 and β9) and four strands (β4, β6, β7 and β8) (Fig. 1a). The core β-sheets are surrounded by four α-helices and loops. A small loop (1283–1286) was not built as the electron density for that region was completely missing. Overall, the TNKS-1 PARP domain structure is similar to the previously reported crystal structures of PARP-enzymes.[2,19] In comparison with PARP-1,[20] the principal secondary structure features (nine β-strands and four α-helices) of TNKS-1 are conserved (Fig. 1b). One of the helices, α2, is longer in TNKS-1 than in PARP-1. The region surrounding the PARP catalytic core, however, shows significant variability (Fig. 2a). The most striking feature, already known based on the sequence, is that the N-terminal α-helical domain of PARP-1 is completely missing in TNKS-1. This domain is thought to modulate the activity of DNA-dependent PARPs.[2,22] Another large deletion in comparison with PARP-1 is on the backside of the catalytic domain where a 32-amino-acid loop (952–984, B-loop) (Fig. 2a) is replaced by a small loop in which four residues were disordered in the present crystal structure. Loops at the analogous position are thought to participate in substrate specificity of mono(ADP-ribosyl)ating toxins.[23]

Despite the conservation of secondary-structure elements, there are large differences in the loop structures, which are of potential functional importance. Most interestingly, the TNKS-1 catalytic domain has a short zinc-binding motif, which is present only in tankyrases and not in other member of the PARP-family (see below).

Lastly, TNKS-1 and TNKS-2 are very similar in domain organization as well as in sequence. For the catalytic domain presented here the sequence identity between TNKS-1 and TNKS-2 is 89% (Fig. 1b). Mapping the variable residues onto the TNKS-1 structure (Fig. 1a) shows that all differences are located far away from the active site, as expected for enzymes catalyzing the same reaction with the same substrate proteins.

Active site, implications for inhibitor design

The PARP catalytic domain contains two distinct binding sites referred to as the donor and acceptor sites (Fig. 1a). In the initiation reaction, when NAD^+ is first added to a glutamate of a target protein, NAD^+ occupies the donor site. This donor site has been mapped based on the similarity with mono(ADP-ribosyl)ating toxins.[2] During the initiation reaction the target protein must occupy the acceptor site in order to position itself for the reaction. In the elongation reaction the donor site is occupied by NAD^+ and the acceptor site is occupied by the growing poly (ADP-ribose) (PAR) chain. The only structural evidence for the acceptor site so far has been the observation of a poorly defined fragment of a NAD^+ analog in a crystal structure of PARP-1.[24] The "catalytic triad" of PARPs is defined by an HYE motif near the donor nicotinamide binding site (NI subsite), although this motif is not completely conserved within the family.[25] The triad His1184-Tyr1213-Glu1291 is, however, conserved in tankyrases as is the rest of the NI subsite.

All of the current PARP inhibitors, at least those for which structural information is available, mimic the NI motif and thus target the NI subsite, with different extensions towards the rest of the donor site.[20,21,26] This mode of interaction is confirmed in all PARP-1 complex structures published to date. The main interactions that are shared between NAD^+ and PARP inhibitors are stacking between two tyrosine residues (Tyr1213 and 1224) and hydrogen bonds with the backbone carbonyl and amide of Gly1185 and side chain of Ser1221. Many attempts to identify novel PARP-1 inhibitors have been made and the patent literature is abundant.[27,28]

In the following we compare the TNKS-1 structure with two representative PARP-1 structures in complex with inhibitors, for which we generated improved structural models based on the existing experimental data (see Materials and Methods). It is apparent that the features that are key for inhibitor binding to the NI subsite are conserved also in TNKS-1 (Fig. 1b). However, the regions lining the adenosine (AD) subsite of the donor site are different in TNKS-1 and PARP-1 and may thus provide a route for design of selective inhibitors. In particular, the D-loop F1197–G1211 has low sequence conservation and displays a different conformation in TNKS-1. This loop adopts an open conformation in all PARP-1 structures, whereas it adopts a closed conformation in the TNKS-1 structure (Fig. 2b). In fact, the inhibitors visible in the PARP-1 structures[20,21] sterically clash with the TNKS-1 D-loop when overlaid (Fig. 2b). The TNKS-1 D-loop has higher temperature factors than the protein on average and is thus likely to be flexible. We propose that upon NAD^+ or inhibitor binding this loop may adopt a conformation similar to that of the PARP-1 apo structure. However, due to its low sequence

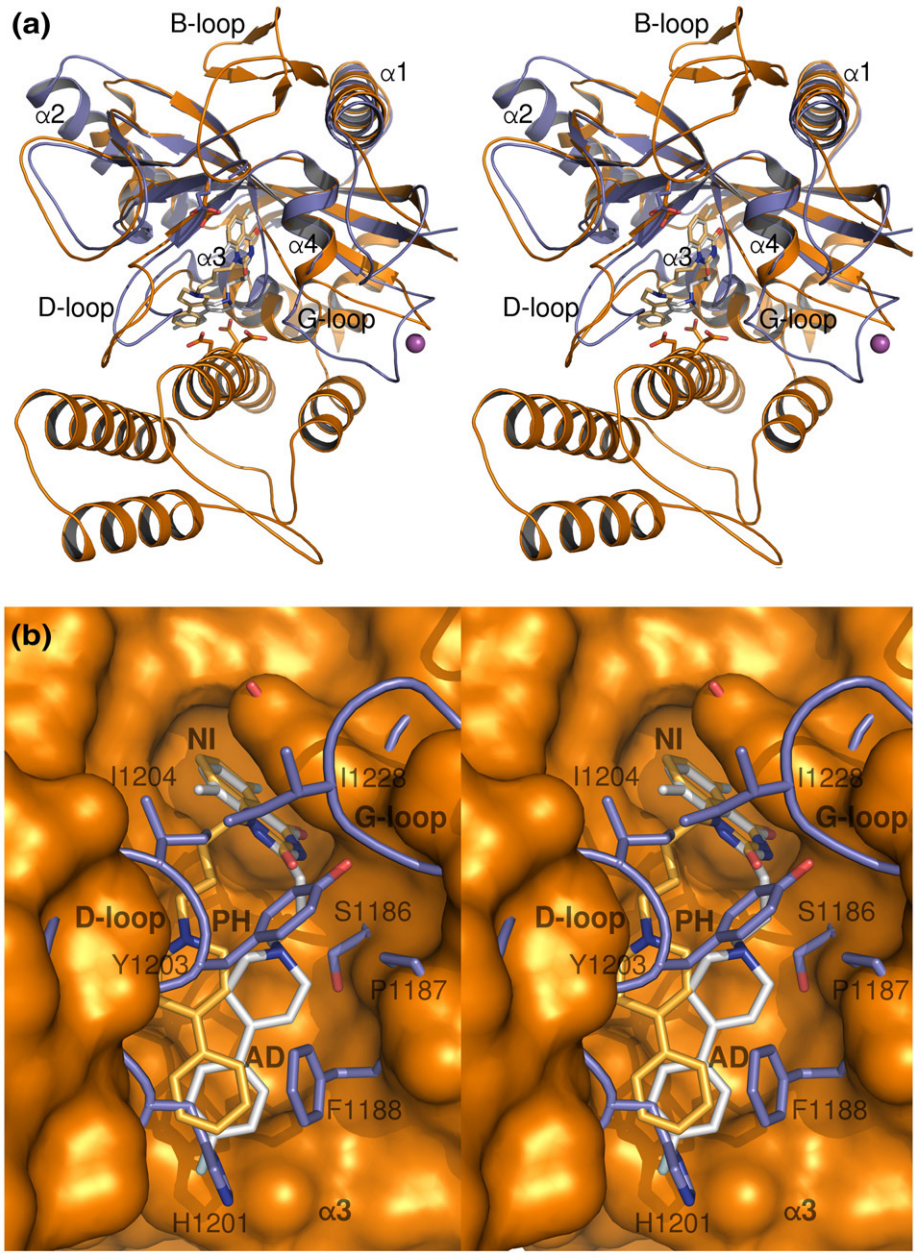

Fig. 2. Comparison of TNKS-1 and PARP-1. (a) Superposed human TNKS-1 and PARP-1 (re-refined 1UK1;see Materials and Methods). Aligned residues are also shown in Fig. 1b. The catalytic glutamate (1291) is shown as sticks as are the residues of PARP-1 N-terminal domain that are suggested to participate in NAD^+ binding.[2] The zinc ion is shown as a sphere. The helices of TNKS-1 are labeled as in Fig. 1a. Inhibitors bound to the PARP-1 structures are shown as sticks: 5-fluoro-1-[4-(4-phenyl-3,6-dihydropyridin-1(2*H*)-yl)butyl]quinazoline-2,4(1*H*,3*H*)-dione in 1UK1 (orange)[20] and FR257517 in 1UK0 (grey).[21] The donor-site loop, which changes conformation upon NAD^+ binding (D-loop), a loop missing in TNKS-1 but present in PARP-1 (B-loop) and the glycine-rich loop (G-loop) are labeled. (b) Closed donor site. Surface of PARP-1 (1UK1) is shown in orange as in (a), but it was calculated without the N-terminal domain. TNKS-1 is shown in blue to emphasize the almost complete closure of this binding site in TNKS-1. Subsites for NAD^+ binding are labeled: NI, nicotinamide-binding site; PH, phosphate-binding site; AD, adenosine-binding site. The AD site is partly occupied by a glycerol molecule in TNKS1. Inhibitors are shown as in (a). Residues closing the donor site in TNKS1 are shown as sticks and labeled, as are the structural features lining the donor site (B-loop, D-loop and α3).

conservation, the interactions with the adenosine part of NAD^+, or inhibitors binding in this site, cannot be fully conserved. Interestingly, a loop at this region is thought to control the substrate specificity of mono-ribosylating toxins.[23] It is also noteworthy that the similar active-site loop gets disordered or changes conformation in diphtheria toxin and in *Pseudomonas* exotoxin A upon NAD^+ binding.[29,30] Moreover, the helix α3 provides a base for the AD subsite *via* interactions with its main-chain atoms.[24] This helix is slightly shorter in TNKS-1 due to the insertion of a proline (Pro1187) and deletion of a two-amino-acid residue, causing movement of the helix and the preceding loop, which results in a narrower binding pocket (Fig.

2b). In a similar manner as for the D-loop, steric clashes are observed when the PARP-1 inhibitor complex [Protein Data Bank (PDB) code 1UK0] is superposed with the TNKS-1 structure (Fig. 2b). Although the structure must change upon NAD^+ or inhibitor binding, the steric clash between Phe1188 and the inhibitor is striking and thus inhibitors designed for PARP-1 and binding to this site may not inhibit TNKS-1. The same clashes described above are observed also using the original published coordinates of 1UK0 and 1UK1 (Supplementary Fig. 1). It should also be noted that the movement of the glycine-rich loop (G-loop; Fig. 2) following α4 also results in a slightly narrower NI site that could also potentially affect binding of NI mimics. The G-loop also connects the zinc-binding motif to the active site of TNKS-1 (see below).

Taken together, these observations point to opportunities for the design of selective TNKS inhibitors. The conserved interactions in the NI site provide an anchor, and it should be possible to base the development of future TNKS inhibitors on the many binding scaffolds identified for PARP-1. In fact, many PARP-1 inhibitors have been used to inhibit also TNKS-1.[17] By extending existing scaffolds by novel substitutions probing the AD subsite, it should be possible to find unique interactions with non-conserved D-loop residues in particular. This situation is very much analogous to what is observed for protein kinase inhibitors; for example, a number of highly conserved interactions are shared by many inhibitors, yet it is possible to identify reasonably selective compounds by proper substitutions.[31]

Zinc-binding motif

Surprisingly, the loop formed by residues 1224–1247 contains a novel, not previously predicted zinc-finger-like motif. According to the sequence alignment, the zinc-binding motif is unique to TNKS-1 and TNKS-2 and is not present in any other PARP enzyme.[25] The presence of zinc in the metal-binding site was suggested by the tetrahedral coordination by mainly cysteines, typical for zinc ions,[32,33] and was confirmed by X-ray fluorescence emission spectra and energy absorption spectra (data not shown). The zinc ion is coordinated by three cysteines (Cys1234, Cys1242 and Cys1245) and one histidine (His1237) (Figs. 1b and 3a). The loop of four residues between the zinc-binding residues (His1237 and C1242) turns back towards the protein (Fig. 3a). Two hydrophobic residues (Tyr1243 and Ile1244) between the last two cysteines (Cys1242 and Cy1245) attach the loop structure to the main body of the protein. Between TNKS-1 and TNKS-2 there is only one amino acid substitution in the Zn-binding loop sequence: Thr1236 is a valine in TNKS-2 (Fig. 1). The Thr1236 side chain is on the outer side of the loop pointing towards the solvent (Fig. 3a) and thus this change should not affect the conformation of the loop or zinc binding. The zinc atom in TNKS-1 is located 33 Å from the catalytic Glu1291, making it very unlikely that it participates directly in catalysis (Fig. 1a). It is also 20 Å away from the closest parts of the donor NAD^+ binding site. This indicates that the zinc-binding motif may be a structural element needed for protein stability or it may have a regulatory function.

A SPASM search[35,36] to find structural motifs in the PDB similar to the loop Cys1234–Cys1245 did not identify any homologous motifs, but when only the Zn-coordinating residues were used, SPASM found nine similar unique entries in the PDB. All entries contain a zinc ion, and although the coordinating residues are at similar positions, only structures of RING-type zinc fingers display the same order of coordinating residues. Ring fingers are not structurally related to the zinc finger in TNKS-1, as the connecting loop in the RING fingers is significantly longer[37]—between 17 and 22 residues in the hits found by SPASM. Interestingly, the SPASM search identified motifs differing in sequence, but of a length similar to that found in TNKS-1. These short motifs can be grouped into the class of "short zinc-binding motifs".[38] In the short zinc-binding motifs, at least three of the four zinc-coordinating residues belong to the same short loop. According to Krishna *et al.*, this group comprises 12 motifs belonging to two families composed of sequences where all four Cys/His residues are found in the same loop (family I) and motifs where one of the coordinating residues is separated in the primary amino acid sequence (family II).[38] The TNKS-1 zinc-binding loop clearly belongs to family I of short zinc-binding loops as the whole motif consists of only 12 residues. Family I consists of nucleotide interacting proteins (1CYQ, 1I3Q, 1A5T and 1GPC) and metabolic enzymes (1HSO and 1E3J). Notably, none of the identified short zinc-binding loops appear to be catalytically important, but are involved in forming protein–protein interactions[39–43] or have a purely structural role in stabilizing the protein fold.[44]

Biological function of the zinc-binding motif

Based on a BLAST search, the zinc-binding motif is conserved among species except in one isoform of *Mus musculus* TNKS-1 (EDL35447), where the zinc-binding loop is completely deleted. Although this gene sequence might be just an error in sequencing, it is interesting that TNKS-1 is suggested not to interact with TRF1 in *M. musculus*.[45] Due to its conservation among species it appears that the zinc-binding motif is of functional importance. Although the zinc ion is located far away from the active site, it is connected to the donor site *via* the G-loop, and it could modulate the activity through this protein backbone link.

Many of the classic zinc fingers function through DNA binding and contain a highly basic/polar area that participates in binding to the DNA backbone.[46] The electrostatic potential of the TNKS-1 zinc-binding motif is positive (Fig. 3b), indicating that it could interact with a negatively charged partner, such as nucleic acids. Although DNA has been reported to increase TNKS-1 activity in some experiments,[47] the authors concluded that DNA would not modulate the activity of TNKS-1 because this was not seen reproducibly. Indeed it is not known what signal, or

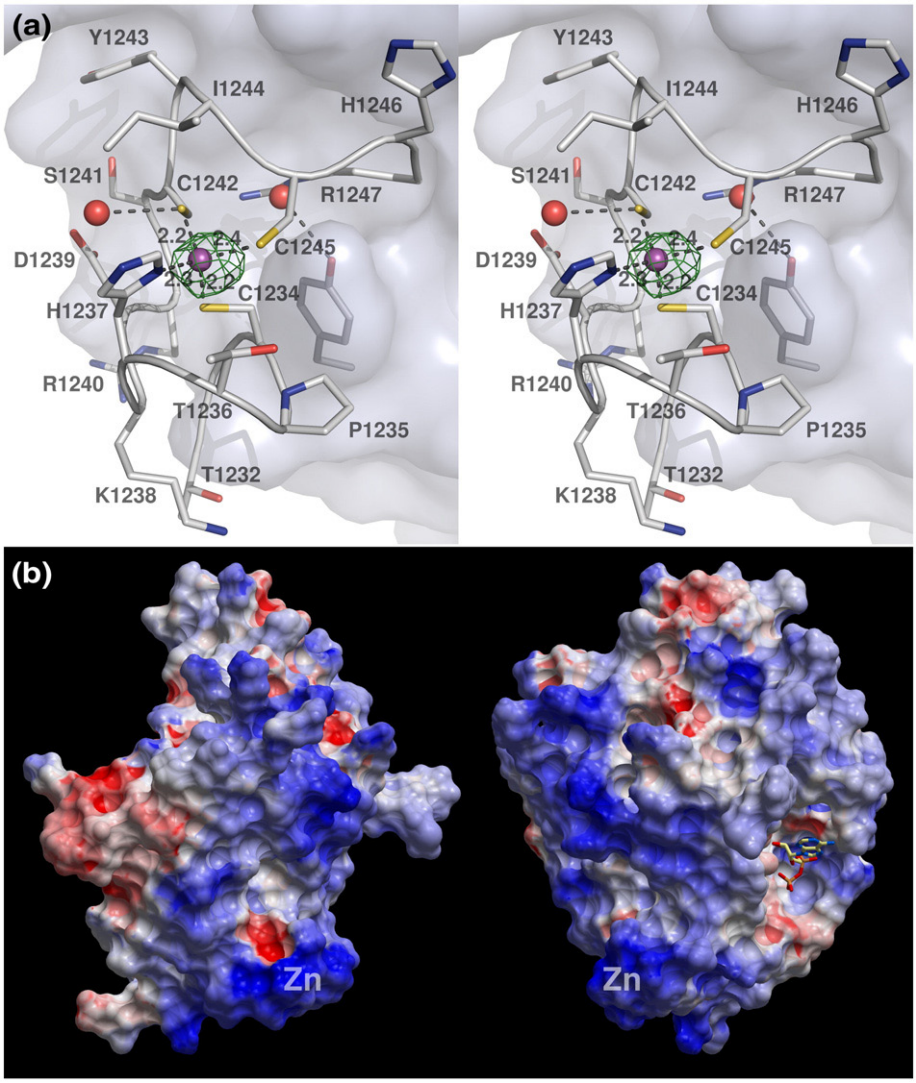

Fig. 3. The zinc-binding motif in TNKS-1 (a) The loop containing the zinc-binding residues is shown. The zinc ion (magenta) and the two water molecules (red) closest to the zinc ion are shown as spheres. Hydrogen bonds to zinc and water molecules by the side chains are drawn as dashed lines. Distances are in angstroms. The anomalous map is contoured in green at 4 σ (0.10 e/Å^3). The molecular surface of TNKS-1, excluding the zinc loop, is shown in light blue. The figure was made with Pymol.[34] (b) The electrostatic surface of TNKS-1. Colour coding of the molecular surface goes from red (−5 kcal/e.u. charge) to blue (+5 kcal/e.u. charge). Zn^{2+} was included in the calculations and the zinc-binding loop is labeled with "Zn". Carba-NAD in PARP-1 (1A26) is shown as a stick model to indicate the acceptor site. Two views of the molecule, 90° apart, are shown.

signals, trigger the TNKS-1 activity; however, a zinc-binding motif could act as a platform for interaction with DNA or an acidic protein molecule. The positive charge around the zinc-binding motif is typical for DNA-binding zinc fingers and thus it should not yet be excluded that DNA, under some circumstances, could activate TNKS-1. Recently zinc fingers have been reported to function also as PAR-binding motifs[48]; this would be a possible and interesting function for the zinc-binding motif of tankyrases.

Concluding remarks

The analysis of the TNKS-1 structure in light of the existing structural knowledge of other PARP enzymes and PARP inhibitors shows that there is clearly potential for the development of selective TNKS-1 inhibitors. By making proper substitutions on existing or novel scaffolds targeting the PARP NI site, it should be possible to identify compounds that have specific interactions, in particular with the non-conserved D-loop. Although we cannot present a clear function for the zinc-binding motif of TNKS-1, it is tempting to propose that it could form a platform for interactions with some of the protein components of the shelterin complex, e.g., by providing a binding site for TIN2, which is known to stabilize the TNKS-1–TRF1 complex and prevent PARsylation of TRF1.[49] TRF1 binds to the C-terminal subdomain of the ankyrin domain of TNKS-1 being separated by a sterile alpha motif domain from the PARP-domain[50]; thus, TIN2 could participate in this interplay of the domains by modulating the activity in a similar fashion as the helical domain of PARP-1.

Materials and Methods

Cloning and protein expression

The TNKS-1 gene clone was obtained from National Institutes of Health Mammalian Gene Collection (MGC), accession no. BC098394. The sequence encoding residues 1091–1325 was amplified by PCR and inserted into pNIC28-Bsa4 vector by ligation-independent cloning. The MGC clone contains an amino acid difference (in comparison with NCBI sequence NP_003738), M1266I, which is located on the surface of the protein (Fig. 1a). The construct included an N-terminal tag containing 6-His sequence (MHHHHHHSSGVDLGTENLYFQSM). For expression, the pNIC-Bsa4 containing the insert was transformed into *Escherichia coli* Rosetta2(DE3) strain and stored at −80 °C.

Cells from the glycerol stock were streaked on an LB agar plate supplemented with 50 μg/ml kanamycin and 34 μg/ml chloramphenicol and incubated overnight at 37 °C. Several colonies from the plate were used to inoculate 20 ml of Terrific Broth supplemented with 8 g/l glycerol, 100 μg/ml kanamycin and 34 μg/ml chloramphenicol and grown at 30 °C overnight. The 20-ml culture was used to inoculate 1.5 l Terrific Broth media supplemented with 8 g/l glycerol, 50 μg/ml kanamycin, 34 μg/ml chloramphenicol and 5 drops of BREOX (anti-foaming agent) in a 2-l glass flask. Cells were grown in a Large-Scale Expression System at 37 °C until the OD_{600} reached 2. The cultivation was down-tempered to 18 °C for 1 h. Expression of TNKS-1 was induced by the addition of 0.5 mM IPTG and continued overnight at 18 °C. Cells were harvested by centrifugation at 5500*g* for 10 min at 4 °C. The pellet was resuspended in lysis buffer containing 50 mM Hepes (pH 7.5), 300 mM NaCl, 10% glycerol, 10 mM imidazole, 0.5 mM tris(2-carboxyethyl)phosphine (TCEP) and complete ethylenediaminetetraacetic-acid-free protease inhibitor (Roche Biosciences). Resuspended cells were stored at −80 °C.

Protein purification

The frozen cell suspension was thawed and 4 μl of 250 U/μl benzonase (Novagen) was added per 50 ml of suspension. The sample was sonicated on ice (Sonics Vibra-Cell) at 80% amplitude, 4 s on, 4 s off, for 3 min followed by centrifugation at 49,000*g* for 20 min at 4 °C. The soluble fraction was decanted and filtered through a 0.45-μm filter.

Purification was conducted automatically on an ÄKTAxpress system (GE Healthcare) operated by UNICORN. Prior to purification, a 1-ml HiTrap chelating column was equilibrated with buffer 1 (30 mM Hepes, 500 mM NaCl, 10% glycerol, 10 mM imidazole, pH 7.5, 0.5 mM TCEP). A Superdex 75 gel filtration column (HiLoad 16/60, GE Healthcare) was equilibrated with buffer 2 (30 mM Hepes, 300 mM NaCl, 10% glycerol, pH 7.5, 0.5 mM TCEP). The cleared lysate was loaded onto the HiTrap chelating column and the column was washed with buffer 1 followed by a wash with the same buffer supplemented with 25 mM imidazole. Bound protein was eluted from the IMAC columns with buffer 1 containing 500 mM imidazole and loaded onto the gel filtration column run using buffer 2. The UV_{280} absorption chromatogram of the eluate showed one major protein peak at a retention volume of 65 ml, indicating monomeric protein. This peak consisted of TNKS-1 as analyzed by SDS-PAGE and routine electrospray ionization mass spectrometry. Fresh TCEP was added to the pooled protein peak to a final concentration of 2 mM and the protein was concentrated to 22.8 mg/ml (0.28 ml) using an Amicon Ultra 15 (Millipore) centrifugal concentrator with a 10,000 molecular weight cutoff. The preparation was flash-frozen in small aliquots for storage at −80 °C.

Crystallization, data collection and structure determination

TNKS-1 crystals were grown by sitting-drop vapour diffusion. Protein (18.2 mg/ml; 0.2 μl) was mixed with reservoir solution (0.1 μl) containing 18% polyethylene glycol 3350, 180 mM magnesium formate (pH 5.9) and 3% 1,6-hexanediol. The drop was equilibrated at 20 °C over the precipitant solution and rodlike crystals appeared in 3 days.

A crystal was picked up with a nylon loop, dipped into a cryosolution (precipitant solution supplemented with 20% glycerol and 300 mM NaCl) and frozen in liquid nitrogen. Data to 2.3 Å resolution were collected at beamline 14.1 (Bessy, Berlin). As data contained intense ice rings, a lower resolution data (2.6 Å) from identically grown crystals were also collected. Resolution shells of the ice rings were excluded from the higher resolution data and the two data sets were scaled together (Table 1). Data were processed with XDS[52] in space group $I2_12_12_1$ (a=79.95 Å, b=81.24 Å

Table 1. Data and refinement statistics

Data statistics	
Wavelength (Å)	0.97981
Space group	$I2_12_12_1$
Cell dimensions	
a (Å)	79.95
b (Å)	81.24
c (Å)	82.72
Resolution (Å)	20–2.3 (2.4–2.3)
R_{merge} [c]	16.6 (47.0)
$I/\sigma(I)$	13.4 (4.2)
Completeness (%)	97.8 (99.9)
Redundancy	9.0 (7.5)
Unique reflections	12043
Refinement statistics	
R_{work} [a]/R_{free} [b]	0.193/0.250
No. atoms	1767
Protein	1664
Water	96
Zinc	1
Glycerol	6
B-factors (Å^2)	
Protein	24.1
Zinc	27.3
Other	26.9
RMSDs	
Bond lengths (Å)	0.013
Bond angles (°)	1.336
Ramachandran plot (%)[d]	
Favoured	97.5
Additionally allowed	2.5

Values for the highest resolution shell are shown in parentheses.

[a] R_{work} is defined as $\sum||F_{obs}|-|F_{calc}||/\sum|F_{obs}|$, where F_{obs} and F_{calc} are observed and calculated structure-factor amplitudes, respectively.

[b] R_{free} is the R−factor for the test set (8% of the data, 968 reflections).

[c] $R_{merge}=\sum_i|I_i-\langle I\rangle|/\sum\langle I\rangle$, where I is an individual intensity measurement and $\langle I\rangle$ is the average intensity for this reflection with summation over all data.

[d] According to Molprobity.[51]

and $c = 82.72$ Å). The structure was solved with MOLREP[53,54] using PARP-12 (PDB code 2PQF) with truncated side chains as a search model. Model building was done with COOT[55] and refinement with REFMAC5 (Table 1).[56] TLS refinement with three groups was carried out in REFMAC5 with the groups selected according to the suggestion of the TLS motion determination server.[57,58]

Re-refinement of human PARP-1 structures

In order to compare differences between human TNKS-1 and PARP-1, the low-resolution (3 Å) models of human PARP-1 (PDB codes 1UK0,[21] 1UK1[20] and 1WOK[26]) were analyzed using the Molprobity server.[51] It was evident that the geometry of these structural models could be improved, and these structures were therefore first refined against the original diffraction data obtained from the PDB. For 1UK1 and 1UK0, a new test set was created and bias was removed by removing solvent atoms, resetting *B*-factors and running molecular replacement with MOLREP.[53,54] In the first refinement cycles, simulated annealing was used within PHENIX[59] and later refinement cycles were done with REFMAC5.[56] One TLS group per monomer was used with 1UK0 and 1UK1, and for 1WOK the N-terminal helical domain and the PARP domain were defined as separate TLS groups. The re-refinement of the 1UK0 and 1UK1 PARP-1 inhibitor complexes resulted in improved models, as judged by Molprobity.[51] Molprobity scores for the three structures improved from 3.7–4.2 to 2.1–2.5 and the fraction of residues in favoured regions of the Ramachandran plot from 70.5–82.5% to 96.3–97.8%. The improved structures were used in the further analysis. It should also be pointed out that the observed electron density for the inhibitor in 1WOK is poor‡.

Analysis of the structure and alignments

The alignment of TNKS-1 and TNKS-2 was carried out using ClustalW.[60] Structural alignments were done with COOT[55] using the secondary-structure matching based algorithm.[61] The anomalous map (Fig. 3a) was calculated from data scaled without merging the Friedel pairs and using the model coordinates as phase information. All the figures excluding Fig. 3b were generated with Pymol.[34] The electrostatic surface shown in Fig. 3b was calculated using ICM (Molsoft).

Protein Data Bank accession codes

The coordinates and structure factors of TNKS-1 were deposited at the PDB under accession code 2RF5.

Acknowledgements

The Structural Genomics Consortium is a registered charity (no. 1097737) that receives funds from the Canadian Institutes for Health Research, the Canadian Foundation for Innovation, Genome Canada through the Ontario Genomics Institute, GlaxoSmithKline, Karolinska Institutet, the Knut and Alice Wallenberg Foundation, the Ontario Innovation Trust, the Ontario Ministry for Research and Innovation, Merck and Co., Inc., the Novartis Research Foundation, the Swedish Agency for Innovation Systems, the Swedish Foundation for Strategic Research and the Wellcome Trust. We acknowledge BESSY and ESRF for synchrotron radiation facilities and we would like to thank Dr. Heike Richter and Dr. Joanne McCarthy for assistance in using beam lines BL 14.1 and ID-29, respectively.

‡Coordinates for all the re-refined structures are available at http://sgc.ki.se/supp_info/TNKS1

Supplementary Data

Supplementary data associated with this article can be found, in the online version, at doi:10.1016/j.jmb.2008.03.058

References

1. Smith, S., Giriat, I., Schmitt, A. & de Lange, T. (1998). Tankyrase, a poly(ADP-ribose) polymerase at human telomeres. *Science*, **282**, 1484–1487.
2. Ruf, A., de Murcia, G. & Schulz, G. E. (1998). Inhibitor and NAD+ binding to poly(ADP-ribose) polymerase as derived from crystal structures and homology modeling. *Biochemistry*, **37**, 3893–3900.
3. Schreiber, V., Dantzer, F., Amé, J. C. & de Murcia, G. (2006). Poly(ADP-ribose): novel functions for an old molecule. *Nat. Rev. Mol. Cell Biol.* **7**, 517–528.
4. Hsiao, S. J. & Smith, S. (2007). Tankyrase function at telomeres, spindle poles, and beyond. *Biochimie*, **90**, 83–92.
5. De Rycker, M., Venkatesan, R. N., Wei, C. & Price, C. M. (2003). Vertebrate tankyrase domain structure and sterile alpha motif (SAM)-mediated multimerization. *Biochem. J.* **372**, 87–96.
6. De Rycker, M. & Price, C. M. (2004). Tankyrase polymerization is controlled by its sterile alpha motif and poly(ADP-ribose) polymerase domains. *Mol. Cell. Biol.* **24**, 9802–9812.
7. Dynek, J. N. & Smith, S. (2004). Resolution of sister telomere association is required for progression through mitosis. *Science*, **304**, 97–100.
8. Canudas, S., Houghtaling, B. R., Kim, J. Y., Dynek, J. N., Chang, W. G. & Smith, S. (2007). Protein requirements for sister telomere association in human cells. *EMBO J.* **26**, 4867–4878.
9. Nugent, C. I. & Lundblad, V. (1998). The telomerase reverse transcriptase: components and regulation. *Genes Dev.* **12**, 1073–1085.
10. de Lange, T. (2005). Shelterin: the protein complex that shapes and safeguards human telomeres. *Genes Dev.* **19**, 2100–2110.
11. Wright, W. E., Piatyszek, M. A., Rainey, W. E., Byrd, W. & Shay, J. W. (1996). Telomerase activity in human germline and embryonic tissues and cells. *Dev. Genet.* **18**, 173–179.
12. Meyerson, M., Counter, C. M., Eaton, E. N., Ellisen, L. W., Steiner, P., Caddle, S. D. *et al.* (1997). hEST2, the putative human telomerase catalytic subunit gene, is up-regulated in tumor cells and during immortalization. *Cell*, **90**, 785–795.
13. Kim, N. W., Piatyszek, M. A., Prowse, K. R., Harley, C. B., West, M. D., Ho, P. L. *et al.* (1994). Specific

association of human telomerase activity with immortal cells and cancer. *Science*, **266**, 2011–2015.
14. Shay, J. W. & Bacchetti, S. (1997). A survey of telomerase activity in human cancer. *Eur. J. Cancer*, **33**, 787–791.
15. Nakamura, T. M., Morin, G. B., Chapman, K. B., Weinrich, S. L., Andrews, W. H., Lingner, J. *et al.* (1997). Telomerase catalytic subunit homologs from fission yeast and human. *Science*, **277**, 955–959.
16. Zimmermann, S. & Martens, U. M. (2007). Telomeres and telomerase as targets for cancer therapy. *Cell. Mol. Life Sci.* **64**, 906–921.
17. Seimiya, H., Muramatsu, Y., Ohishi, T. & Tsuruo, T. (2005). Tankyrase 1 as a target for telomere-directed molecular cancer therapeutics. *Cancer Cell*, **7**, 25–37.
18. Ratnam, K. & Low, J. A. (2007). Current development of clinical inhibitors of poly(ADP-ribose) polymerase in oncology. *Clin. Cancer Res.* **13**, 1383–1388.
19. Oliver, A. W., Amé, J. C., Roe, S. M., Good, V., de Murcia, G. & Pearl, L. H. (2004). Crystal structure of the catalytic fragment of murine poly(ADP-ribose) polymerase-2. *Nucleic Acids Res.* **32**, 456–464.
20. Hattori, K., Kido, Y., Yamamoto, H., Ishida, J., Kamijo, K., Murano, K. *et al.* (2004). Rational approaches to discovery of orally active and brain-penetrable quinazolinone inhibitors of poly(ADP-ribose)polymerase. *J. Med. Chem.* **47**, 4151–4154.
21. Kinoshita, T., Nakanishi, I., Warizaya, M., Iwashita, A., Kido, Y., Hattori, K. & Fujii, T. (2004). Inhibitor-induced structural change of the active site of human poly(ADP-ribose) polymerase. *FEBS Lett.* **556**, 43–46.
22. Miranda, E. A., Dantzer, F., O'Farrell, M., de Murcia, G. & de Murcia, J. M. (1995). Characterisation of a gain-of-function mutant of poly(ADP-ribose) polymerase. *Biochem. Biophys. Res. Commun.* **212**, 317–325.
23. Sun, J., Maresso, A. W., Kim, J. J. & Barbieri, J. T. (2004). How bacterial ADP-ribosylating toxins recognize substrates. *Nat. Struct. Mol. Biol.* **11**, 868–876.
24. Ruf, A., Rolli, V., de Murcia, G. & Schulz, G. E. (1998). The mechanism of the elongation and branching reaction of poly(ADP-ribose) polymerase as derived from crystal structures and mutagenesis. *J. Mol. Biol.* **278**, 57–65.
25. Otto, H., Reche, P. A., Bazan, F., Dittmar, K., Haag, F. & Koch-Nolte, F. (2005). In silico characterization of the family of PARP-like poly(ADP-ribosyl)transferases (pARTs). *BMC Genomics*, **6**, 139.
26. Iwashita, A., Hattori, K., Yamamoto, H., Ishida, J., Kido, Y., Kamijo, K. *et al.* (2005). Discovery of quinazolinone and quinoxaline derivatives as potent and selective poly(ADP-ribose) polymerase-1/2 inhibitors. *FEBS Lett.* **579**, 1389–1393.
27. Curtin, N. J. (2005). PARP inhibitors for cancer therapy. *Expert Rev. Mol. Med.* **7**, 1–20.
28. Peukert, S. & Schwahn, U. (2004). New inhibitors of poly(ADP-ribose) polymerase (PARP). *Exp. Opin. Ther. Patents*, **14**, 1531–1551.
29. Bell, C. E. & Eisenberg, D. (1996). Crystal structure of diphtheria toxin bound to nicotinamide adenine dinucleotide. *Biochemistry*, **35**, 1137–1149.
30. Li, M., Dyda, F., Benhar, I., Pastan, I. & Davies, D. R. (1996). Crystal structure of the catalytic domain of *Pseudomonas* exotoxin A complexed with a nicotinamide adenine dinucleotide analog: implications for the activation process and for ADP ribosylation. *Proc. Natl Acad. Sci. USA*, **93**, 6902–6906.
31. Manley, P. W., Cowan-Jacob, S. W., Buchdunger, E., Fabbro, D., Fendrich, G., Furet, P. *et al.* (2002). Imatinib: a selective tyrosine kinase inhibitor. *Eur. J. Cancer*, **38**, S19–S27.
32. Harding, M. M. (2000). The geometry of metal–ligand interactions relevant to proteins. II. Angles at the metal atom, additional weak metal–donor interactions. *Acta Crystallogr.* **56**, 857–867.
33. Harding, M. M. (2001). Geometry of metal–ligand interactions in proteins. *Acta Crystallogr., Sect. D: Biol. Crystallogr.* **57**, 401–411.
34. DeLano, W. L. (2002). The PyMOL Molecular Graphics System. DeLano Scientific, Palo Alto, CA.
35. Kleywegt, G. J. (1999). Recognition of spatial motifs in protein structures. *J. Mol. Biol.* **285**, 1887–1897.
36. Madsen, D. & Kleywegt, G. J. (2002). Interactive motif and fold recognition in protein structures. *J. Appl. Crystallogr.* **35**, 137–139.
37. Gamsjaeger, R., Liew, C. K., Loughlin, F. E., Crossley, M. & Mackay, J. P. (2007). Sticky fingers: zinc-fingers as protein-recognition motifs. *Trends Biochem. Sci.* **32**, 63–70.
38. Krishna, S. S., Majumdar, I. & Grishin, N. V. (2003). Structural classification of zinc fingers: survey and summary. *Nucleic Acids Res.* **31**, 532–550.
39. Jelokova, J., Karlsson, C., Estonius, M., Jornvall, H. & Hoog, J. O. (1994). Features of structural zinc in mammalian alcohol dehydrogenase. Site-directed mutagenesis of the zinc ligands. *Eur. J. Biochem.* **225**, 1015–1019.
40. Banfield, M. J., Salvucci, M. E., Baker, E. N. & Smith, C. A. (2001). Crystal structure of the NADP(H)-dependent ketose reductase from *Bemisia argentifolii* at 2.3 Å resolution. *J. Mol. Biol.* **306**, 239–250.
41. Cramer, P., Bushnell, D. A. & Kornberg, R. D. (2001). Structural basis of transcription: RNA polymerase II at 2.8 ångström resolution. *Science*, **292**, 1863–1876.
42. Guenther, B., Onrust, R., Sali, A., O'Donnell, M. & Kuriyan, J. (1997). Crystal structure of the delta' subunit of the clamp-loader complex of *E. coli* DNA polymerase III. *Cell*, **91**, 335–345.
43. Galburt, E. A., Chevalier, B., Tang, W., Jurica, M. S., Flick, K. E., Monnat, R. J., Jr. & Stoddard, B. L. (1999). A novel endonuclease mechanism directly visualized for I-PpoI. *Nat. Struct. Biol.* **6**, 1096–1099.
44. Shamoo, Y., Friedman, A. M., Parsons, M. R., Konigsberg, W. H. & Steitz, T. A. (1995). Crystal structure of a replication fork single-stranded DNA binding protein (T4 gp32) complexed to DNA. *Nature*, **376**, 362–366.
45. Muramatsu, Y., Ohishi, T., Sakamoto, M., Tsuruo, T. & Seimiya, H. (2007). Cross-species difference in telomeric function of tankyrase 1. *Cancer Sci.* **98**, 850–857.
46. Lee, M. S., Gippert, G. P., Soman, K. V., Case, D. A. & Wright, P. E. (1989). Three-dimensional solution structure of a single zinc finger DNA-binding domain. *Science*, **245**, 635–637.
47. Cook, B. D., Dynek, J. N., Chang, W., Shostak, G. & Smith, S. (2002). Role for the related poly(ADP-ribose) polymerases tankyrase 1 and 2 at human telomeres. *Mol. Cell. Biol.* **22**, 332–342.
48. Ahel, I., Ahel, D., Matsusaka, T., Clark, A. J., Pines, J., Boulton, S. J. & West, S. C. (2008). Poly(ADP-ribose)-binding zinc finger motifs in DNA repair/checkpoint proteins. *Nature*, **451**, 81–85.
49. Ye, J. Z. & de Lange, T. (2004). TIN2 is a tankyrase 1 PARP modulator in the TRF1 telomere length control complex. *Nat. Genet.* **36**, 618–623.
50. Seimiya, H., Muramatsu, Y., Smith, S. & Tsuruo, T. (2004). Functional subdomain in the ankyrin domain of tankyrase 1 required for poly(ADP-ribosyl)ation of TRF1 and telomere elongation. *Mol. Cell. Biol.* **24**, 1944–1955.

51. Lovell, S. C., Davis, I. W., Arendall, W. B., 3rd, de Bakker, P. I., Word, J. M., Prisant, M. G. *et al.* (2003). Structure validation by Calpha geometry: phi, psi and Cbeta deviation. *Proteins*, **50**, 437–450.
52. Kabsch, W. (1993). Automatic processing of rotation diffraction data from crystals of initially unknown symmetry and cell constants. *J. Appl. Crystallogr.* **26**, 795–800.
53. CCP4. (1994). The CCP4 suite: programs for protein crystallography. *Acta Crystallogr., Sect. D: Biol. Crystallogr.* **50**, 760–763.
54. Vagin, A. & Teplyakov, A. (1997). MOLREP: an automated program for molecular replacement. *J. Appl. Crystallogr.* **30**, 1022–1025.
55. Emsley, P. & Cowtan, K. (2004). Coot: model-building tools for molecular graphics. *Acta Crystallogr., Sect. D: Biol. Crystallogr.* **60**, 2126–2132.
56. Murshudov, G. N., Vagin, A. A. & Dodson, E. J. (1997). Refinement of macromolecular structures by the maximum-likelihood method. *Acta Crystallogr., Sect. D: Biol. Crystallogr.* **53**, 240–255.
57. Painter, J. & Merritt, E. A. (2006). Optimal description of a protein structure in terms of multiple groups undergoing TLS motion. *Acta Crystallogr., Sect. D: Biol. Crystallogr.* **62**, 439–450.
58. Painter, J. & Merritt, E. A. (2006). TLSMD web server for the generation of multi-group TLS models. *J. Appl. Crystallogr.* **39**, 109–111.
59. Adams, P. D., Grosse-Kunstleve, R. W., Hung, L. W., Ioerger, T. R., McCoy, A. J., Moriarty, N. W. *et al.* (2002). PHENIX: building new software for automated crystallographic structure determination. *Acta Crystallogr., Sect. D: Biol. Crystallogr.* **58**, 1948–1954.
60. Thompson, J. D., Higgins, D. G. & Gibson, T. J. (1994). CLUSTAL W: improving the sensitivity of progressive multiple sequence alignment through sequence weighting, position-specific gap penalties and weight matrix choice. *Nucleic Acids Res.* **22**, 4673–4680.
61. Krissinel, E. & Henrick, K. (2004). Secondary-structure matching (SSM), a new tool for fast protein structure alignment in three dimensions. *Acta Crystallogr., Sect. D: Biol. Crystallogr.* **60**, 2256–2268.